Thermodynamic fluctuations in canonical shock-turbulence interaction

Yogesh Prasaad M. S.

Department of Aerospace Engineering
Indian Institute of Technology Bombay
Mumbai, 400076, India
yogesh@aero.iitb.ac.in

Krishnendu Sinha

Department of Aerospace Engineering
Indian Institute of Technology Bombay
Mumbai, 400076, India
krish@aero.iitb.ac.in

Johan Larsson

Department of Mechanical Engineering
University of Maryland
College Park, MD, 20742, USA
jola@umd.edu

ABSTRACT

In this work, we use direct numerical simulation and linear interaction analysis to study the thermodynamic field generated by the interaction of a shock wave with homogeneous isotropic turbulence. Fluctuations in density, pressure, temperature and entropy can play an important role in shock-induced mixing, combustion and energy transfer processes. Data from high-fidelity simulations is used to investigate the variation of thermodynamic fluctuations with flow Mach number for a constant turbulent Mach number and Reynolds number. As expected, density, pressure and temperature variances attain large values at the shock, followed by, in general, a decaying profile in the downstream flow. There are, however, cases with non-monotonic variation with Mach number as well as local peaks in density fluctuations behind the shock. These are explained in terms of the contribution of the post-shock acoustic and entropy modes and their cross-correlation to the thermodynamic variances. Budget of the transport equations reveal interesting insight into the physics governing the trends observed behind the shock wave. It is found that the downstream evolution of the thermodynamic field is determined by competing dilatational and dissipation mechanisms. The dominant mechanisms are identified for a range of conditions and their implication for developing predictive models is highlighted.

INTRODUCTION

Shock waves are characteristic features in compressible flows, specifically in the supersonic/hypersonic flow regime. In aerospace applications, the effect of shock waves on the turbulent features in a supersonic boundary layer is usually studied to understand the physical mechanisms responsible for boundary layer separation, increased heat transfer and high surface pressures, each of which are unique engineering problems. The interaction of free turbulence with a planar shock wave is a similar problem of interest, exhaustive with physical insights on the effects of shock on turbulence and vice-versa without additional complexities of mean shear, streamline curvature, wall effects, etc. Shock-turbulence interaction has implications in a variety of applications, to name a few, supersonic/hypersonic propulsion systems, inertial confinement fusion, shock wave lithotripsy, and astrophysical shock waves. In this study, we focus on the interaction of a homogeneous/isotropic turbulence interacting with a nominally planar shock wave, which is the most basic form of shock-turbulence interaction.

Initial studies of shock-turbulence interaction were theoretical, mostly employing linear analysis and are based on the Kovásznay (1953) decomposition of turbulence. The theory aptly called as the linear interaction analysis (LIA) was developed by Moore (1954) and Ribner (1954) to analyze the interaction of acoustic and vorticity waves respectively with an unsteady normal shock. The theory was later put to use by many researchers to study problems involving shocks and free turbulence (e.g., Mahesh *et al.* (1996), Fabre *et al.* (2001), Wouchuk *et al.* (2009), Quadros *et al.* (2016*b*)). Physical experiments utilizing grid-generated turbulence interacting with a normal shock have also been carried out (cf. Agui *et al.* (2005) and references therein) to study the underlying mechanisms responsible for amplification of turbulent kinetic energy (TKE) and the modification of length scales across the shock; purely driven by the need to understand mixing enhancement across the shock and shock wave/turbulent boundary layer interaction (SBLI). Several numerical simulations have been carried out to study the canonical shock-turbulence interaction problem due to its geometric simplicity and rich physics (e.g., Lee *et al.* (1997); Larsson *et al.* (2013); Ryu & Livescu (2014)), with the focus of understanding the amplification of turbulent kinetic energy and enstrophy, reduction in length scales, and enhanced anisotropy in post-shock Reynolds stresses.

Compressible turbulent flows are characterized by the appreciable changes in thermodynamic quantities such as density, pressure and temperature fluctuations, which can be drastically amplified/altered on interaction with shock waves. The importance of understanding the thermodynamic fluctuations is well known as they play a major role in turbulent mass flux, sound generation, turbulent heat flux, and most importantly, in the turbulent transport of energy between internal and kinetic energy components.

The objective of the present study is to perform a detailed investigation of the thermodynamic aspects of the canonical shock-turbulence interaction. This work attempts to explain the amplification and evolution mechanisms of thermodynamic fluctuations in canonical shock-turbulence interaction by systematic variation of the governing parameters in the direct numerical simulations (DNS): flow Mach number (M), turbulent Mach number (M_t) and Taylor-scale Reynolds number (Re_λ). The physical mechanisms behind the variations in thermodynamic quantities are understood using LIA and the extensive DNS data of Larsson *et al.* (2013). Additional numerical simulations have been carried out to supplement the existing data. A controlled study is carried out with purely vortical incoming turbulence in LIA and mostly vortical with minimal compressible fluctuations in the DNS data.

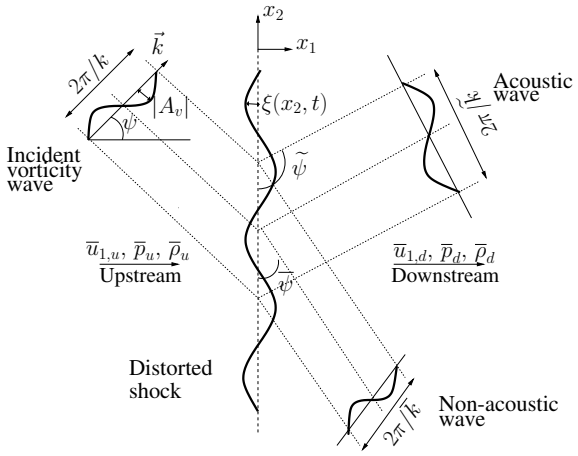

Figure 1: Schematic of a single vorticity wave interacting with a normal shock and yielding acoustic, entropy and vorticity waves downstream of the shock wave.

METHODOLOGY

We use LIA and DNS to study the problem of a homogeneous/isotropic turbulence (HIT), being convected by a uniform one-dimensional (1D) mean flow and interacting with a planar normal shock. Cartesian coordinate system is used where the shock-normal direction is represented by x_1 and the shock-parallel directions by x_2 and x_3. We use the notion of Favre averages (density-weighted) for all quantities from the numerical simulations except for density (ρ) and pressure (p). The Favre averages are denoted as $\widetilde{f}$ and the associated fluctuations are given by double primes. In LIA, we use Reynolds averaged quantities denoted by an overbar and their respective fluctuations denoted by single primes. When comparing results between LIA and DNS, we make use of the assumption $\widetilde{f} \approx \overline{f}$ (linear limit). The upstream and downstream states are denoted by subscripts 'u' and 'd' respectively.

Linear theory

A single vorticity wave in two-dimensions (x_1, x_2) of amplitude A_v and at an angle ψ with the x_1-direction is being convected by a 1D uniform mean flow of velocity $\overline{u}_{1,u}$ towards the normal shock as shown in Fig. (1). The shock deforms in response and the position of the unsteady shock is given by $\xi(x_2,t)$. The downstream non-acoustic waves (entropy and vorticity) are generated/refracted at an angle $\overline{\psi}$ and are convected as 'frozen' waves by the downstream mean flow with velocity $\overline{u}_{1,d}$. The acoustic waves are generated at an angle $\widetilde{\psi}$ and are either propagating or decaying (reduction in amplitude), depending on whether the angle of the incident wave is lower or higher than the critical angle.

The complete details of the LIA procedure can be obtained from Mahesh *et al.* (1996), Quadros *et al.* (2016*b*) and Livescu & Ryu (2016). In brief, the linearized Euler equations are used to obtain the waveforms of the fluctuations in the upstream and downstream regions of the normal shock wave (modeled as a discontinuity). Linearized Rankine-Hugoniot (RH) conditions are used as the boundary conditions at the shock wave to obtain the transfer functions of the post-shock fluctuations. The upstream turbulence is represented as a super-position of 2D plane waves (Fourier modes), with each of them independently interacting with the shock. The post-shock field thus obtained is then integrated over all of the incident waves in a specified energy spectrum (von Kármán) to obtain a statistical description of the turbulence behind the shock wave. It is to be noted that the upstream turbulence considered in LIA is purely vortical with no thermodynamic fluctuations.

Numerical simulations

The compressible Navier-Stokes (NS) equations are solved for a perfect gas with ratio of specific heats $\gamma = 1.4$ and zero bulk viscosity using the solution-adaptive finite difference *Hybrid* code (Larsson *et al.* (2013)). A linear relationship is used for relating the viscous stresses (σ_{ij}) to the strain rates and Fourier's law is used for the heat flux (q_j). Viscosity is assumed to follow a power-law with temperature as $\mu = \mu_{ref}(T/T_{ref})^{3/4}$. The homogeneous/isotropic turbulence is generated as per the method given in Larsson *et al.* (2013) with the initial turbulent field specified using the von Kármán velocity spectrum having peak energy wavenumber of $k_0 = 4$. The isotropic databases are temporally decayed till 'realistic' turbulence is obtained, followed by a blending of multiple realizations to form a sufficiently long database that satisfies statistical convergence. Taylor's hypothesis is used to convect the blended database as the time-dependent inflow turbulence for the shock-turbulence interaction domain. The inflow turbulence used in the numerical simulations is quasi-vortical with minimal amount of thermodynamic and compressible fluctuations. The turbulence parameters immediately upstream of the shock are: turbulent Mach number $M_{t,u} = 0.15$, Taylor-scale Reynolds number of $Re_{\lambda,u} = 33$ and dissipation-scale Reynolds number $Re_{L_{\varepsilon,u}} \approx 135$.

Simulations with four different upstream Mach numbers ($M_u = 1.23, 1.50, 2.50$ and 3.50) have been carried out in the present study. The computational grid is stretched in the shock-normal direction (x_1) to facilitate finer grid sizes near the shocks. A uniform grid spacing in used for the shock-parallel directions (x_2 and x_3). The grid sizes are varied to ensure that the anisotropically compressed post-shock turbulence is captured as the shock strength varies between the cases. An optimized numerical sponge is attached at the end of the domain to gradually dissipate the spurious oscillations from the outflow. A non-reflecting outflow boundary condition and a back pressure controller to adjust the mean shock position are setup according to the method provided in Larsson & Lele (2009). The present case details are tabulated in table (1) and the simulations have been validated by comparing with the available data of Larsson *et al.* (2013). We note that the current simulations have grid resolution comparable to the viscous shock thickness for the low Mach number cases and vary by a factor of $4-5$ for the high Mach number cases.

Table 1: List of cases simulated in the present study

M_u	$L_{\varepsilon,u}/\eta_u$[1]	$\Delta x_{1,s}/\Delta x_{2/3}$[2]	δ/η[3]	Grid
1.23	45	0.75	0.90	882×384^2
1.50	45	0.50	0.41	1042×384^2
2.50	46	0.40	0.14	1142×384^2
3.50	46	0.33	0.08	1313×384^2

[1] Ratio of dissipation length scale to Kolmogrov length scale - a measure of turbulence Reynolds number

[2] Ratio of shock-normal grid size at the shock to that of the shock-parallel grid size - a measure of grid resolution at the shock

[3] Estimate for viscous shock thickness taken from Ryu & Livescu (2014): $\delta/\eta \approx 7.69 M_{t,u}/(\sqrt{Re_{\lambda,u}}(M_u - 1))$

RESULTS AND DISCUSSIONS

We compare thermodynamic variances ($\overline{\rho'^2}$, $\overline{p'^2}$, $\overline{T'^2}$, $\overline{s'^2}$) obtained from DNS and LIA. We discuss the spatial variation of the thermodynamic fluctuations first, followed by a discussion on the effect of upstream Mach number. Kovásznay type mode decomposition is followed to split the thermodynamic variances into their respective elementary modes as given in Quadros *et al.* (2016*a*). This enables to understand the underlying linear mechanisms in the amplification of the thermodynamic fluctuations.

We have normalized the thermodynamic variances by the square of their mean downstream values ($\overline{\rho}_d^2$ / $\overline{p}_d^2$ / $\overline{T}_d^2$) except for entropy. Entropy variance is normalized by the square of the gas specific heat capacity at constant pressure (c_p^2). Additionally, the variances are normalized by the ratio of upstream turbulent kinetic energy to the square of the upstream mean shock-normal velocity ($0.5M_t^2/M^2$) so as to remove the effect of upstream turbulence intensity. We normalize the streamwise direction by the peak energy wavenumber (k_0). This normalization procedure is used throughout this article, unless otherwise specified. The shock-normal direction in numerical simulations is shifted such that the mean shock location (identified as the location where the mean dilatation is most negative) is aligned with the mean shock location in LIA, i.e., centered at $k_0x_1 = 0$.

Spatial variation

The thermodynamic variances shown in figure 2 have almost negligible values in the flow upstream of the shock wave. They exhibit a jump to relatively high values across the shock, followed by a rapid decay in the downstream flow, except entropy, which instead shows a gradual decay. In DNS, the interaction yields locally high values of the fluctuations in the shock region, which are due to the unsteady oscillation of the shock wave and do not represent turbulence.

Thermodynamic fluctuations predicted by LIA are comparable to that obtained from the DNS for low Mach numbers ($M_u < 2$), mainly due to the 'nearly isentropic' nature of the post-shock field for these shock strengths. At the higher Mach numbers ($M_u > 2$), there is a significant generation of entropy fluctuations. The density variance shows a non-monotonic variation behind the shock, similar to that of the shock-normal Reynolds stresses. This is also observed in LIA till the acoustic adjustment region ($k_0x_1 \lesssim 2$), beyond which there are differences between DNS and LIA due to the viscous decay (which is not considered in the LIA framework). DNS pressure fluctuations appear to approach a finite asymptotic value in the far-field ($k_0x_1 \to \infty$) and is comparable to that obtained from LIA. The fact that there are pressure fluctuations that are unaffected by viscous decay is entirely consistent with the notion that the shock produces a far-field radiating sound field. There is a slight mismatch in $\overline{p'^2}$ in the region immediately behind the shock (around $k_0x_1 = 1$) indicating the effect of the non-linear mechanisms in DNS; however, the effect is minimal.

The temperature variances in DNS show a rapid decay immediately behind the shock, similar to the inviscid decay of the pressure fluctuations and a gradual decay approximately after the acoustic adjustment region ($k_0x_1 \gtrsim 1$). LIA, on the other hand, predicts the rapid decay after the post-shock amplification but followed by a constant far-field value after the adjustment region. The post-shock entropy fluctuations as predicted by LIA match the DNS values obtained immediately behind the shock, but do not reproduce the viscous decay observed in DNS in the downstream region.

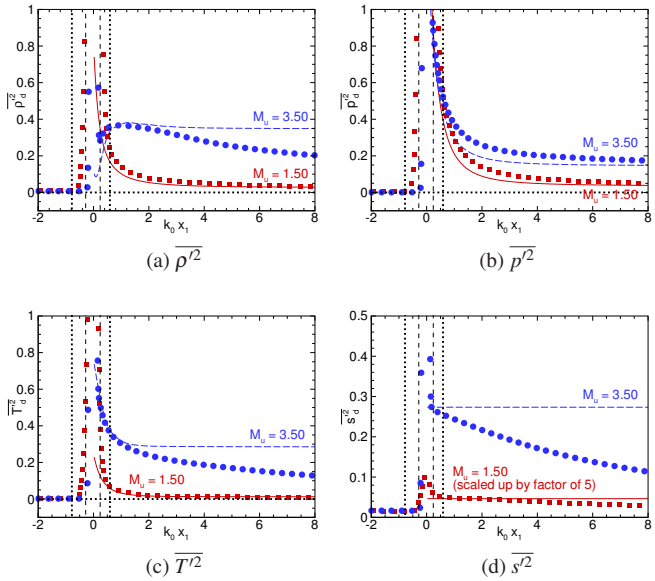

Figure 2: Spatial variation of the thermodynamic variances for $M_u = 1.5$ (red - solid lines and squares) and 3.5 (blue - dashed lines and circles). Lines represent LIA solution and symbols represent DNS results taken from present simulations. Vertical dotted and dashed lines represent the bounds of the mean shock thickness for $M_u = 1.5$ and $M_u = 3.5$ cases respectively. Note that the entropy variance generated by the $M = 1.5$ shock is scaled up by a factor of 5 to appear in the same plot.

Kovásznay modes

The Kovásznay modes of entropy and acoustics (or pressure) are fundamentally different in terms of their evolution behind the shock wave. The majority of the acoustic energy decays with distance from the shock wave; in particular, those associated with the single-wave interactions exceeding the critical angle. On the other hand, the entropy mode generated at the shock propagates downstream without any change in amplitude as per the linear inviscid framework adopted by LIA.

The LIA solution in the post-shock region is a superposition of acoustic, entropy and vorticity waves, with a collection of orientation angles and wavelengths. The density variance is thus (since the pure vorticity contribution, $\rho'_{d,v} = 0$),

$$\overline{\rho'_d\rho'_d} = \overline{(\rho'_{d,a}+\rho'_{d,e})^2} = \overline{\rho'_{d,a}\rho'_{d,a}} + \overline{\rho'_{d,e}\rho'_{d,e}} + 2\overline{\rho'_{d,a}\rho'_{d,e}} \qquad (1)$$

which allows us to decompose the full density variance into a pure acoustic contribution ("acoustic-acoustic", the first term), a pure entropy contribution ("entropy-entropy", the second term), and a combined acoustic/entropy contribution ("acoustic-entropy", the third term). A similar decomposition is done for the temperature variance.

Figure 3 shows the components of density and temperature variance for the low shock strength ($M_u = 1.5$) and the high shock strength ($M_u = 3.5$) cases. The "acoustic-acoustic" component in both the variances has large values immediately behind the shock and decay in the streamwise direction, similar to $\overline{p'^2}$. The "acoustic-entropy" correlation also shows a decaying pattern and vanishes beyond the acoustic adjustment region ($0 < k_0x_1 \gtrsim 1$). The "entropy-entropy" component is constant with the streamwise direction, and

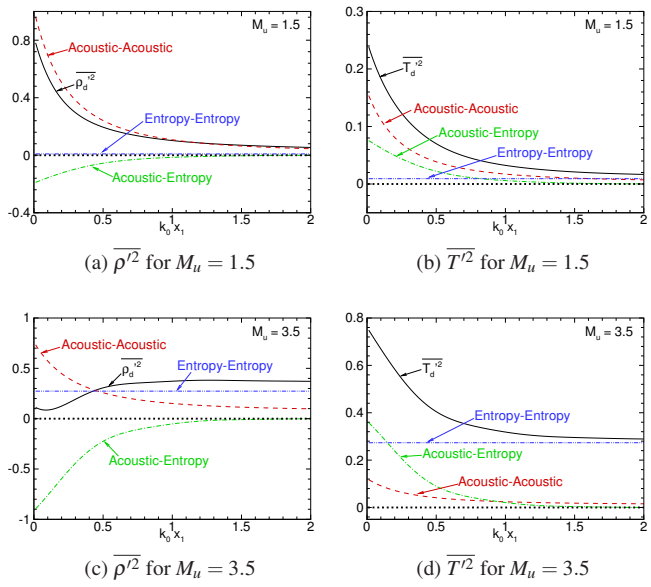

(a) $\overline{\rho'^2}$ for $M_u = 1.5$ (b) $\overline{T'^2}$ for $M_u = 1.5$

(c) $\overline{\rho'^2}$ for $M_u = 3.5$ (d) $\overline{T'^2}$ for $M_u = 3.5$

Figure 3: Spatial variation of the Kovásznay type modal components in $\overline{\rho_d'^2}$ and $\overline{T_d'^2}$ from LIA.

is relatively small in magnitude for the low Mach number case, such that the far-field density and temperature variances are mostly due to the contribution of the propagating acoustic waves.

Data plotted for the Mach 3.5 interaction in figure 3 (c, d) shows a significantly large contribution of the entropy mode to the density and temperature variances. The far-field values of $\overline{\rho'^2}$ and $\overline{T'^2}$ are primarily determined by the "entropy-entropy" component, which is once again invariant with distance from the shock. All the components are positive for the temperature fluctuations, and they together give a monotonic decay of $\overline{T'^2}$ to its far-field value. On the other hand, the "acoustic-entropy" component in $\overline{\rho'^2}$ is of opposite sign when compared to its counterpart in the temperature fluctuations. The total contribution of the "acoustic-acoustic" and the "entropy-entropy" is balanced by the largely negative "acoustic-entropy" term in the acoustic adjustment region resulting in a non-monotonic variation to its far-field value.

The "acoustic-acoustic" component in density variance differ by a factor of $(\gamma-1)^2$ and the "acoustic-entropy" component is by a factor of $(\gamma-1)$ against their respective counterparts in the temperature variance, indicating that LIA assumes the post-shock field to be isentropic, even for high Mach numbers.

Effect of shock strength

We next plot the post-shock thermodynamic variances as a function of upstream Mach number in figure 4 at a particular location using the data from Larsson *et al.* (2013) (squares and diamonds), the present simulations (circles) and LIA (lines). For a constant turbulent Mach number and Reynolds number, the underlying trend in the DNS data against Mach number can be identified using LIA. The variation of far-field values against Mach number is usually of interest however, DNS and LIA solutions vary in the far-field due to the effects of viscous dissipation in DNS. In this regard, we choose the location $k_0x_1 = 1$, where the "acoustic-entropy" correlation almost vanishes in LIA and does not have significant effects of the viscous terms in DNS. This location is in the rapidly decaying portion of the post-shock thermodynamic field, in between the near-field ($k_0x_1 = 0^+$) and far-field ($k_0x_1 = \infty$) values predicted by LIA, and is able to bring out the quantitative trends in the variation of the thermodynamic variances with Mach numbers.

As expected, the thermodynamic variances show a monotonic increase with Mach number, i.e. a stronger shock generates higher amplitudes of thermodynamic fluctuations. All thermodynamic variances computed from DNS follows the LIA prediction closely for the entire range of shock strengths. There are, however, quantitative differences between the solutions for the pressure and density variances, due to the effect of non-linear mechanisms in that location (see figure 2 (b)). There are large variations between LIA and DNS results as the turbulent Mach number is increased, and a good match between the two when the Reynolds number is increased, which is in agreement with the assumptions of LIA.

Pressure fluctuations appear to quickly rise to a finite value even for weak interactions ($M_u < 1.5$) and then saturate at high Mach numbers. The post-shock entropy fluctuations appear to increase as the square of the upstream Mach number. As a result, they attain small values for weak shock interactions and rapidly increase with Mach number beyond 2. The density and temperature variances show a variation which is a combination of the acoustic and the entropy fluctuations. This is distinct in the density fluctuations (LIA data) where the variation is similar to the pressure fluctuations for $M_u < 1.65$ and follows the trend of the entropy fluctuations for $M_u > 2$. The DNS data (see the variation of $M_{t,u} = 0.22$ data) also follows this trend obtained from LIA.

The near-field thermodynamic variances (obtained from LIA) are also plotted against Mach number in figure 4. Near-field density variances attain a peak value at low Mach numbers ($M_u \approx 1.2$) and reduce in amplitude as the shock strength increases, till they vanish at very high Mach numbers. Near-field values of pressure variances show a similar trend, except that they saturate to a constant value at very high Mach numbers. Temperature variances are found to be monotonically increasing as the shock strength increases in the near-field region, and have values larger than at the k_0x_1 location. LIA predicts entropy fluctuations to be spatially invariant and thus the trend is observed to be the same as $k_0x_1 = 1$ location.

Transport of the variances

The physical mechanisms underlying the post-shock evolution of the thermodynamic variances is next analyzed in terms of the budgets of their respective transport equations. The transport equations are obtained by multiplying the thermodynamic fluctuations with their respective transport equation, followed by a suitable averaging process. The complete transport equations for the variances can be found in Gerolymos & Vallet (2014). For completeness, the transport of pressure variance is given in equation (2),

$$\underbrace{\partial_t(\overline{p'^2})}_{\text{Temporal}} + \underbrace{\partial_{x_j}(\widetilde{u}_j\overline{p'^2})}_{\text{Convection}} = \underbrace{-\partial_{x_j}(\overline{p'^2u''_j}) + 2(\gamma-1)[\partial_{x_j}(\overline{p'q_j})]}_{\text{Diffusion}}$$
$$\underbrace{-2\overline{p'u''_j}\partial_{x_j}\overline{p} - 2(\gamma-1)\overline{p'^2}\partial_{x_j}\widetilde{u}_j + 2(\gamma-1)\overline{p'\sigma_{ij}}\partial_{x_j}\widetilde{u}_i}_{\text{Production}}$$
$$\underbrace{-2\gamma\overline{p}\,\overline{p'\partial_{x_j}u''_j} - (2\gamma-1)\overline{p'^2\partial_{x_j}u''_j}}_{\text{Dilatation}}$$
$$\underbrace{-2(\gamma-1)\overline{q_j\partial_{x_j}p'}}_{\text{Dissipation}} + \underbrace{2(\gamma-1)\overline{p'\sigma_{ij}\partial_{x_j}u''_i}}_{\text{Triple correlations}} \tag{2}$$

The other variances also do have similar terms such as diffusion by velocity fluctuations, production due to mean gradients, correlations

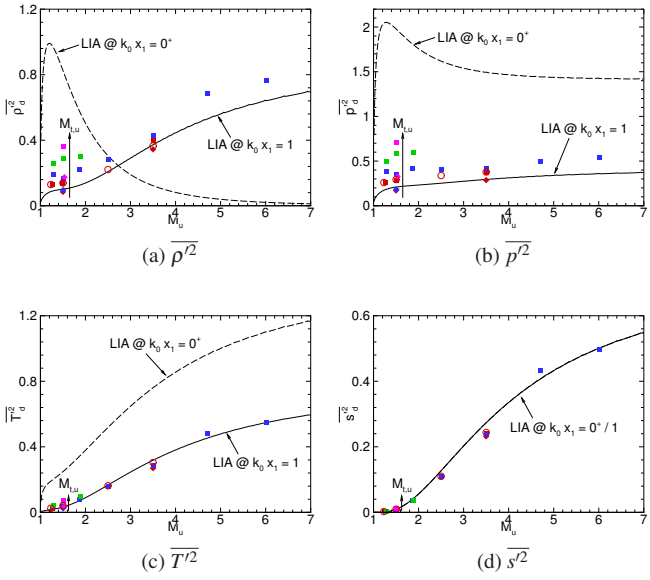

(a) $\overline{\rho'^2}$ (b) $\overline{p'^2}$

(c) $\overline{T'^2}$ (d) $\overline{s'^2}$

Figure 4: Variation of thermodynamic variances against Mach number at the locations, $k_0x_1 = 1$ and the near-field $k_0x_1 = 0^+$ (only for LIA). Squares ($Re_{\lambda,u} = 40$) and diamonds ($Re_{\lambda,u} = 75$) are from the data of Larsson *et al.* (2013) and circles ($Re_{\lambda,u} = 33$) are from the present simulations. Color legend: $M_{t,u} = 0.15/0.16$ (red), $M_{t,u} = 0.22$ (blue), $M_{t,u} = 0.31$ (green), $M_{t,u} = 0.38$ (pink).

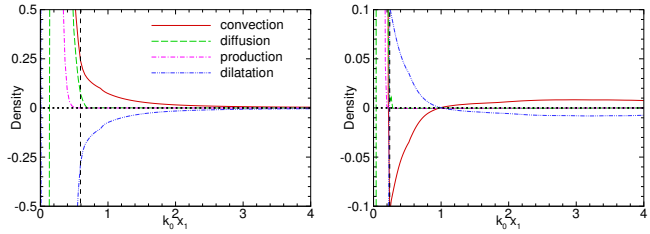

(a) $M_u = 1.50$ (b) $M_u = 3.50$

Figure 5: Budgets of all terms in the transport equation of $\overline{\rho'^2}$ from the present simulations for the Mach numbers: (a) $M_u = 1.50$ and (b) $M_u = 3.50$. The variances and the shock-normal direction are normalized as mentioned in the text and the spatial gradient is normalized by the factor $k_0\overline{u}_{1,u}$. Vertical dashed lines (around $k_0x_1 = 0.3$) represent the downstream edge of the mean shock.

with fluctuating dilatation, and triple correlations.

Figure 5 shows the budget of the terms in the transport equation of the density variance for two shock strengths, computed as part of the current work. The convection of density variance ($\widetilde{u}\partial_{x_1}\overline{\rho'^2}$) is found to be balanced by the correlation of density fluctuations with the fluctuating dilatation ($\overline{\rho'\partial_{x_j}u_j''}$). It is found that the other terms (production, diffusion, and triple correlations) do not have significant contribution in the budget. It is to be noted that transport of density variance does not have any viscous dissipation terms.

The DNS data shown in figure 6 (a) corresponds to the transport of pressure variance where, the correlation of dilatation with pressure is found to be the dominant term, similar to density variance. On the other hand, the DNS data shows that the entropy variance to be governed by dissipation mechanisms only. Figure 6 (b) shows the balancing of the convection of entropy variance by its dissipation term ($\overline{(q_j/T)\,\partial_{x_j}s''}$) for all Mach numbers. Entropy variance is not affected by the acoustic mode and thus, does not have any dilatational correlations.

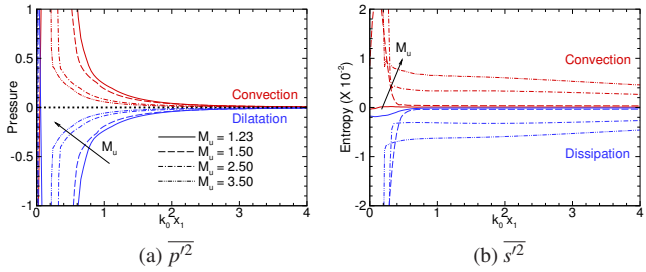

(a) $\overline{p'^2}$ (b) $\overline{s'^2}$

Figure 6: Budgets of the dominant terms in the transport equation of (a) $\overline{p'^2}$ and (b) $\overline{s'^2}$ for four different Mach numbers. Normalization is as mentioned in the caption of figure 5.

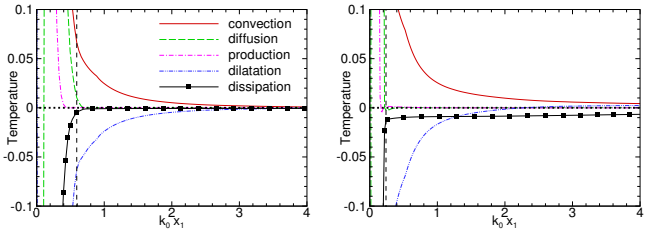

(a) $M_u = 1.5$ (b) $M_u = 3.5$

Figure 7: Budgets of all terms in the transport equation of $\overline{T'^2}$ for Mach numbers: $M_u = 1.50$ and $M_u = 3.50$. The variances are normalized as mentioned in the caption of figure 5. Vertical dashed lines (around $k_0x_1 = 0.3$) represent the downstream edge of the mean shock.

Transport of temperature variances is governed by dilatational correlations at all Mach numbers, according to the DNS data. Figure (7) shows the dominant terms in the budget of temperature variance, where it is found that the dissipation term has a small but finite contribution to the budget at high Mach numbers. Similar to other variances, the contribution of production, diffusion, and third order correlation terms are insignificant.

SUMMARY

In this work, we presented a comparison of the thermodynamic fluctuations generated by canonical shock-turbulence interaction between LIA and DNS. A large parameter space including a range of Mach number, turbulent Mach number and Reynolds number is considered, and available DNS data is complemented with new cases computed here. The linear interaction analysis based on Kovásznay mode decomposition of the disturbances is applied under the linear inviscid framework and is further used to investigate the thermodynamic field in terms of their component Kovásznay modes.

It has been known that pressure, density and temperature fluctuations are produced in a shock-turbulence interaction and they decay rapidly in the downstream flow. This is primarily associated with the acoustic mode, and reciprocates the exponential de-

cay of the acoustic energy generated at the shock. 'Representative' far-field values show steady increase in magnitude with increasing strength of interaction. This is essentially due to the entropy mode contributions to the density and temperature fluctuations. There are interesting non-monotonic trends, for example, in the variation of the near field $\overline{p'^2}$ and $\overline{\rho'^2}$ values with Mach number. The density variance generated by strong shocks ($M \geq 2.5$) also show a non-monotonic variation (and a local peak in magnitude) with distance from the shock wave. These are caused by the interplay between acoustic and entropy modes generated by the interaction.

Transport equations are written to investigate the evolution of the thermodynamic variances downstream of the shock interaction. DNS data is used to compute the budget of the source terms for a range of Mach numbers. We identified that the transport of the thermodynamic variances in the post-shock region to be dominated by dilatational and dissipative mechanisms. The transport equations can be approximated to a suitable degree in the form of,

$$\widetilde{u}\partial_{x_1}\overline{\rho'^2} \approx -2\overline{\rho}\overline{\rho'\partial_{x_j}u''_j}, \tag{3}$$

$$\widetilde{u}\partial_{x_1}\overline{p'^2} \approx -2\gamma\overline{p}\overline{p'\partial_{x_j}u''_j}, \tag{4}$$

$$\widetilde{u}\partial_{x_1}\widetilde{T''^2} \approx -(2/c_v)\overline{p}\overline{T''\partial_{x_j}u''_j} - (2/c_v)\overline{q_j\partial_{x_j}T''}, \tag{5}$$

$$\widetilde{u}\partial_{x_1}\widetilde{s''^2} \approx -2\overline{(q_j/T)\partial_{x_j}s''} \tag{6}$$

where, c_v is the gas specific heat capacity at constant volume.

Dilatation effect is found to be the primary source term for the transport of $\overline{\rho'^2}$, $\overline{p'^2}$ and $\widetilde{T''^2}$ at low Mach numbers. Transport equations for the thermodynamic variances obtained from the linearized inviscid equations also show that the dilatation correlation to be the only source term balancing the convective term without any dissipative mechanisms. The dilatation term can be modeled effectively using the exponential decay of acoustic energy generated by the shock wave. A differential equation model to predict the post-shock variation of $\overline{p'^2}$ can be derived using LIA. A similar approach is expected to work for $\overline{\rho'^2}$ and $\widetilde{T''^2}$ at low Mach numbers where the contribution of entropy component is small. The extensive data presented for $\overline{\rho'^2}$, $\overline{p'^2}$, $\overline{T'^2}$ will be valuable for the model validation.

ACKNOWLEDGEMENTS

YP thank the C-DAC NPSF PARAM YUVA-II supercomputing facility located at Pune, India for providing the required computational resources to run the simulations and post-process the DNS solutions. JL is supported by the National Science Foundation, grant CBET-1453633.

REFERENCES

Agui, J. H., Briassulis, G. & Andreopoulos, Y. 2005 Studies of interactions of a propagating shock wave with decaying grid turbulence: velocity and vorticity fields. *J. Fluid Mech.* **524**, 143–195.

Fabre, D., Jacquin, L. & Sesterhenn, J. 2001 Linear interaction of a cylindrical entropy spot with a shock. *Phys. Fluids* **13** (8), 2403–2422.

Gerolymos, G. A. & Vallet, I. 2014 Pressure, density, temperature and entropy fluctuations in compressible turbulent plane channel flow. *J. Fluid Mech.* **757**, 701–746.

Kovásznay, L. S. G. 1953 Turbulence in Supersonic Flow. *J. Aeronaut. Sci.* **20** (10), 657–674,682, reprinted in *AIAA J.*, **41(7)**, 219–237, 2003.

Larsson, J., Bermejo-Moreno, I. & Lele, S. K. 2013 Reynolds–and Mach–number effects in canonical shock–turbulence interaction. *J. Fluid Mech.* **717**, 293–321.

Larsson, J. & Lele, S. K. 2009 Direct numerical simulation of canonical shock/turbulence interaction. *Phys. Fluids* **21** (12), 1–12.

Lee, S., Lele, S. K. & Moin, P. 1997 Interaction of isotropic turbulence with shock waves: effect of shock strength. *J. Fluid Mech.* **340**, 225–247.

Livescu, D. & Ryu, J. 2016 Vorticity dynamics after the shock–turbulence interaction. *Shock Waves* **26** (3), 241–251.

Mahesh, K., Moin, P. & Lele, S. K. 1996 The interaction of a shock wave with a turbulent shear flow. *Tech. Rep.* TF–69. Thermosciences Division, Department of Mechanical Engineering, Stanford University, Stanford, California 94305.

Moore, F. K. 1954 Unsteady oblique interaction of a shock wave with a plane disturbance. *Tech. Rep.* NACA TR 1165.

Quadros, R., Sinha, K. & Larsson, J. 2016*a* Kovasznay Mode Decomposition of Velocity–Temperature Correlation in Canonical Shock–Turbulence Interaction. *Flow, Turbul. and Combust.* **97** (3), 787–810.

Quadros, R., Sinha, K. & Larsson, J. 2016*b* Turbulent energy flux generated by shock/homogeneous–turbulence interaction. *J. Fluid Mech.* **796**, 113–157.

Ribner, H. S. 1954 Convection of a pattern of vorticity through a shock wave. *Tech. Rep.* NACA TR 1164.

Ryu, J. & Livescu, D. 2014 Turbulence structure behind the shock in canonical shock–vortical turbulence interaction. *J. Fluid Mech.* **756**.

Wouchuk, J. G., Huete Ruiz de Lira, C. & Velikovich, A. L. 2009 Analytical linear theory for the interaction of a planar shock wave with an isotropic turbulent vorticity field. *Phys. Rev. E* **79** (6), 1–35.